MMC-Based Traction System with Regenerative Braking

Vitor Chagas
Universidade de Lisboa,
Instituto Superior Técnico,
Lisboa, Portugal,
vitor.chagas@tecnico.ulisboa.pt

Sónia Pinto
Universidade de Lisboa,
Instituto Superior Técnico,
Lisboa, Portugal,
soniafp@tecnico.ulisboa.pt

***Abstract* — This paper aims to study a railway traction system powered at AC single phase 25kV-50Hz whose operation is based on a controlled modular multilevel converter (MMC). It simulates an on-board system, which receives the power from the grid through the catenary.**

A transformer is used to lower the grid voltage. The MMC converts the 1φ-AC voltage from the transformer to a 3φ-AC voltage which is applied to the induction motor. The 6-level converter consists of 10 submodules within its arms and each submodule is composed by a half-bridge inverter with 2 levels of output voltage. The incoming current is controlled by a linear control, which uses Phase-Shifted Carrier Pulse-With Modulation (PSC-PWM) to activate the semiconductors.

The motor has a V/f constant soft-start and its speed is reduced to validate the bidirectionality of the MMC for regenerative braking.

For the validation of the system dimensioning, all results are graphically demonstrated through simulation using *Matlab/Simulink*.

***Keywords:* Modular Multilevel Converter (MMC); Controller; Bidirectionality; Transformer; Induction Motor.**

I. INTRODUCTION

Rail transportation systems are sorely needed for integration into the modern world. The development of the electrification of these systems provided several advantages such as greater speed, greater safety, less environmental impact and greater capacity.

Table 1 shows the main existing systems of railway electrification used specially in European countries [1].

Table 1 – Railway Electrification Systems

System	Voltage Operation	Distance between Substations
DC	3 kV	Medium
DC	1,5 kV	Medium
DC	0.6 – 1,4 kV	Low
1φ- AC	15 kV - 16,7 Hz 25 kV - 50 Hz	High
3φ - AC	25 kV – 50 Hz	High

Although DC power supplies are still very used in short distance applications, such as metro systems, the importance of AC supplies at industrial frequency is more interesting for long distance applications demanding high-speed trains. [1].

The usage of 25 kV-50 Hz power supplies has become increasingly popular in several countries as the improvement of high-power converters has enabled independence of power to the type of traction motor. Rail electrified at 25kV-50Hz systems provide several advantages when compared to other systems [2]:

- Smallest cross section of overhead conductors;
- Possibility to regenerate energy by braking;
- Lower maintenance cost;
- Simpler design of substations;
- Greater starting efficiency.

II. PROPOSED SYSTEM

Figure 1 shows the proposed traction system which is composed by a transformer, a MMC and the induction motor.

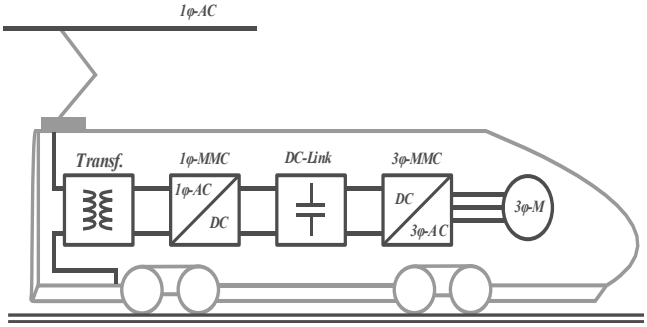

Figure 1 – Traction Vehicle with the Proposed System.

A. Transformer

The 1-φ 25 kV from the grid is lowered through a high-power transformer whose parameters are presented in table 2.

Table 2 – Transformer Parameters.

Definition	Parameter	Value
Rated Power	S_a	700 kVA
Primary Voltage	V_p	25 kV
Secondary Voltage	V_s	4 kV
No-load losses	P_0	0.29%
Full-load losses	P_{sc}	1.43%
Magnetizing current	I_M	1,0%

The current in the secondary of the transformer is the input of the MMC and it is controlled to reach peak value of 260A.

B. Modular Multilevel Converter (MMC)

The MMC was used in this system due to its benefits such as modularity, high efficiency, output waveforms with low harmonic distortion rate, scalability for higher voltages and power levels, absence of capacitors in the DC stage and low electromagnetic interference [3]

B.1. Structure and Operation

Figure 2 shows a MMC with 3 legs, which are representing the phases of the system. Each leg has a positive (upper) and a negative (lower) arm. The upper arm is connected to the positive terminal of the DC-Link whilst the lower arm is connected to its negative terminal. The inductance L_a in each arm limits both the circulating currents between the phases and the fault currents in the DC stage. The proposed MMC has N=10 submodules (SM) in each leg, which are divided 2 arms with 5 submodules each.

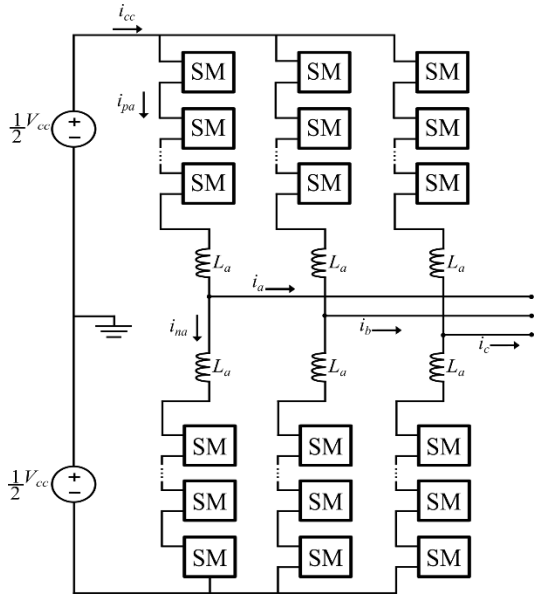

Figure 2 – Three Phase MMC.

The circulating current in a phase is given by:

$$i_{a\_circ} = \frac{i_{pa}}{2} + \frac{i_{na}}{2} - \frac{i_{cc}}{3} \quad (1)$$

The sum of the circulating currents of the three phases is equal to zero.

$$i_{a\_circ} + i_{b\_circ} + i_{c\_circ} = 0 \quad (2)$$

According to the Figure 2, the current in one of the arms can be defined by:

$$i_{pa} = \frac{i_{cc}}{3} + \frac{i_a}{2} + i_{a\_circ} \quad (3)$$

$$i_{na} = \frac{i_{cc}}{3} - \frac{i_a}{2} + i_{a\_circ} \quad (4)$$

Figure 3 shows the half-bridge topology used in each submodule. This topology is composed by two IGBT (insulated-gate bipolar transistor) T_1 and T_2, two antiparallel diodes (D_1 and D_2) to guarantee bidirectional operation and a capacitor C. When the submodule is in ON state, it means the IGBT T_1 is activated and T_2 deactivated. When the submodule is in OFF mode, the IGBT T_1 is disabled and T_2 activated [4].

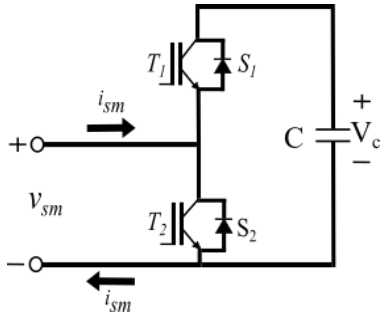

Figure 3 – Half-Bridge Submodule.

Table 3 summarizes the operation of the submodule according to its states of conduction and the effects of current direction on the capacitor.

Table 3 – States of the Submodules and Effects on Current and Capacitor.

State of SM	T_1	T_2	i_{sm}	ΔV_c	v_{sm}
ON	ON	OFF	>0	+	V_c
ON	ON	OFF	<0	-	V_c
OFF	OFF	ON	>0	0	0
OFF	OFF	ON	<0	0	0

The number of ON submodules in the upper arm n_{sON} plus the number of submodules ON in the lower arm n_{iON} is equal to the number of submodules per arm n_i or n_s:

$$n_{sON} + n_{iON} = n_i = n_s \quad (5)$$

Once the submodules are conducting, the voltage in their capacitors is depending on the DC stage and the number of submodules per leg.

$$V_c = \frac{2V_{cc}}{N} \quad (6)$$

The voltage in the arms is depending on the number of submodules which are ON in each arm:

$$v_n = n_{iON} V_c \quad (7)$$

$$v_p = n_{sON} V_c \quad (8)$$

Alternatively, these voltages can be defined per phase by:

$$v_{pabc} = \sum_{k=1}^{n} S_{pabck}\, v_{cabck} \quad (9)$$

$$v_{nabc} = \sum_{k=1}^{n} S_{nabck}\, v_{cabck} \quad (10)$$

$$S = \begin{cases} 0, & SM\ OFF \\ 1, & SM\ ON \end{cases} \quad (11)$$

The intermediate voltage by one of the phases of the converter can be calculated using the following equations:

$$v_{oA} = \frac{V_{cc}}{2} - v_p - L_a \frac{d_{ipA}}{dt} \quad (12)$$

$$v_{oA} = -\frac{V_{cc}}{2} + v_n - L_a \frac{d_{inA}}{dt} \quad (13)$$

B.2. Filter Sizing

As the proposed MMC does not present too many levels, a filter must be sized to reduce the harmonic distortion. The equation (14) shows the maximum inductance for the filter [5].

$$L_f \leq \frac{V_c}{2 f_c (n_m - 1) \Delta i_{Lmáx}} \quad (14)$$

n_m is the number of possible states of each SM.

$\Delta i_{Lmáx}$ is the current variation.

f_c is the switching frequency of the semiconductors.

B.3. Modulation

The technique chosen for this application is the Phase-Shifted Carrier Pulse Width Modulation (PSC-PWM). This option uses a certain number of carriers with same amplitude and offset. This configuration of carriers allows the same duty-cycle for the semiconductors and it helps to distribute their losses equally, which provides greater flexibility and lower harmonic content [6], [7].

Modulation techniques based on PSC-PWM require complementary voltage balancing algorithms in the capacitors, which are related to their charging states. In this study, the submodule capacitors were replaced by DC voltage sources and the techniques for balancing and controlling the voltage in the capacitors can be seen in [8].

A modulation process is composed by a modulator and several carriers that will define the switching states of the sub-modules. For the PSC-PWM used in this study, the carriers are equally time shifted high frequency triangular waves.

The modulator is a nearly sinusoidal wave of fundamental frequency (50Hz) and is compared to carriers, whose respective submodules are conducting when they have a higher value than the modulator.

The phase difference between the carrier p_1 and the carrier p_m can be obtained through the following expression:

$$\phi_{1-m} = (m-1)\frac{T_n}{N} \quad (15)$$

T_n is the switching period and m is the number of the carriers.

The example in Figure 4 has 5 carriers, that are related to 5 SMs. All SMs are ON when the modulator has a lower value than all triangular waves. All submodules are OFF when the modulator device is higher than the carriers. By (15) it can be deduced that the carriers have a 72° phase difference. Figure 5 shows the signal correspondent to the comparison between the modulator and the carriers.

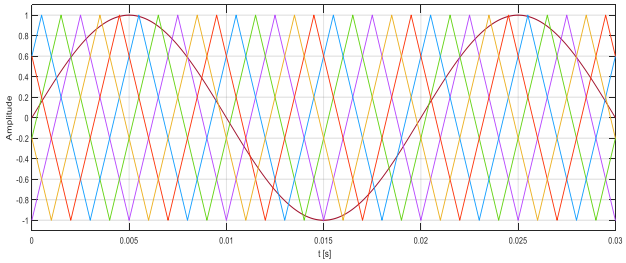

Figure 4 – Modulator and Carriers.

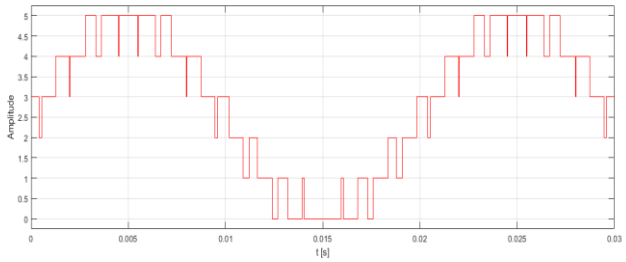

Figure 5 – Comparison Signal Between Carriers and Modulator.

Therefore, the proposed MMC has 6 voltage levels using this modulation technique. The states of the SMs are shown in Table 4, in which SM1 is the upper and SM10 is the lower submodule of the converter's legs.

Table 4 – States of Submodules and Voltage Level of the MMC.

SM1	1	0	0	0	0	0
SM2	1	1	0	0	0	0
SM3	1	1	1	0	0	0
SM4	1	1	1	1	0	0
SM5	1	1	1	1	1	0
SM6	0	1	1	1	1	1
SM7	0	0	1	1	1	1
SM8	0	0	0	1	1	1
SM9	0	0	0	0	1	1
SM10	0	0	0	0	0	1
Voltage Level	+3	+2	+1	-1	-2	-3

B.4. Current Linear Controller

The tool used to control the current which is injected by the grid is the Proportional and Integral Controller (PI), since it guarantees quick response and reduces the error to

almost zero in steady state [5]. This controller is shown Figure 6.

The proportional action ensures that the system reaches the steady state faster and corrects the current proportionally to its error.

The integral part acts through the integration of the error. When the error is positive, it is accumulated and when it is negative, its value is corrected. Hence, steady state error can be nulled.

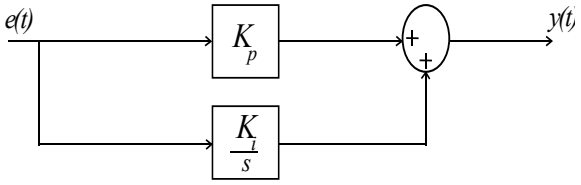

Figure 6 – PI Controller.

The transfer function of the PI controller can be characterized as:

$$H(s) = K_p + \frac{K_i}{s} \quad (16)$$

Where K_p is the proportional gain and K_i is the integral one.

The representation of the (modulation + converter) system can be considered as a first order system with gain K_D and a dominant pole depending on the delay time T_d.

$$T_d = \frac{T_n}{2} \quad (17)$$

$$K_D = \frac{V_{CC}}{u_c máx} \quad (18)$$

$u_c máx$ is the amplitude of the modulator.

The Figure 7 shows the linear control of the current, where α_i represents the gain of the current sensor.

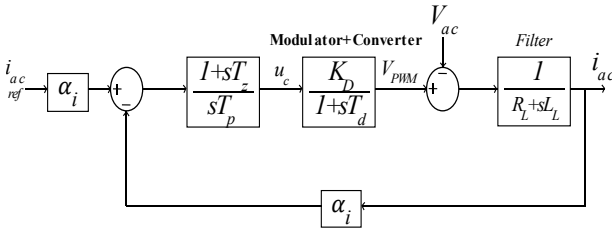

Figure 7 – Linear Control System.

The grid voltage is seen as a disturbance and an equivalent resistance is considered from the controller's reference.

$$R = R_L + \frac{V_{ac}}{i_{ac}} \quad (19)$$

The dynamic zero T_z must coincide with the pole introduced by the input filter, that:

$$T_z = \frac{L_L}{R} \quad (20)$$

Where L_L is the inductance present in the grid.

Therefore, it is possible to obtain the closed loop second order transfer function of the controlled system.

$$G(s) = \frac{i_{ac}(s)}{i_{ac_{ref}}(s)} = \frac{\frac{K_D}{T_p T_d R}}{s^2 + \frac{1}{T_d}s + \frac{K_D \alpha_i}{T_p T_d R}} = \frac{\omega_n^2}{s^2 + 2\xi\omega_n s + \omega_n^2} \quad (21)$$

Considering $\xi = \frac{\sqrt{2}}{2}$ and using equation (20) it is possible to calculate the time T_p:

$$T_p = \frac{2K_D \alpha_i T_d}{R} \quad (22)$$

The proportional and integral gains are obtained through the following equations:

$$K_p = \frac{T_z}{T_p} \quad (23)$$

$$K_i = \frac{1}{T_p} \quad (24)$$

C. Induction Motor

Table 5 presents the parameters of the motor from the proposed system. The three-phase double caged induction motor has a soft-starter, which keeps a constant relation between its voltage and frequency in each phase. The semiconductors from the three legs of the MMC are activated so that the voltage and the frequency fed into the

Table 5 – Induction Motor Parameters.

Definition	Parameter	Value
Nominal power	S_{nom}	110 kVA
Nominal voltage	V_{nom}	400 V_{RMS}
Nominal frequency	f_n	50 Hz
Nominal current	I_{nom}	194 A
Nominal torque	T_{nom}	352 Nm
Synchronous speed	N_{sinc}	3000 rpm
Nominal speed	N_{nom}	2982 rpm
Power Factor	f_p	86%
Pair of poles	p	1
Starting current per nominal current	$\frac{I_{start}}{I_{nom}}$	7.6
Starting torque by nominal torque	$\frac{T_{start}}{T_{nom}}$	2
Stator resistance	R_s	44,34 mΩ
Stator inductance	L_s	234,1 µH
Rotor resistance (inner cage)	R_{r1}	8,114 mΩ
Rotor resistance (inner cage)	L_{r1}	401,7 µH
Rotor resistance (outer cage)	R_{r2}	0.111 Ω
Rotor resistance (outer cage)	L_{r2}	234,1 µH
Mutual inductance	L_m	8,831 mH

motor have the same positive growing rate for a specific time.

The V/f constant driven in motors is performed for speeds lower than synchronous, since the rated motor voltage should not be exceeded. Hence, there is no flow in the motor air gap and the maximum torque is not changed.

The frequency is limited so that there are no torque losses caused by the magnetic flux weakening, which would occur due to the increase of the frequency for a constant voltage.

III. SIMULATION RESULTS

The simulation results of the proposed system from figure 2 are presented in this section. The main features of the system as well as its controller are graphically analysed to guarantee the operation fulfilments imposed by the MMC.

Table 6 show the parameters of the grid, the MMC and controller.

The first simulation is made by increasing the speed and keeping it constant. The second simulation considers a decrease of velocity, which occurs when the train is braking.

Table 6 – Parameters of Grid, MMC and Linear Current Controller

Definition	Parameter	Value
DC Voltage	V_{cc}	10 kV
DC Voltage internal resistance	$2R_{cc}$	2 mΩ
Grid Resistance	R_L	1.5 mΩ
Grid Inductance	L_L	10 mH
Resistance per phase	R_{fase}	0.1 mΩ
Inductance per phase	L_a	100 µH
Voltage in each SM	V_c	2 kV
Semiconductor's Resistance	R_{on}	1 mΩ
Submodules per arm	$\frac{N}{2}$	5
Switching frequency	f_c	10 kHz
Proportional gain	K_p	20
Integral gain	K_i	3077
Zero of linear controller	T_z	$6{,}49*10^{-4}$
Pole of liner controller	T_p	$3{,}24*10^{-5}$
Delay time	T_d	$5{,}0*10^{-5}$
System gain	K_D	50000
Grid Voltage	V_{grid}	25 kV_{RMS}

A. *Increasing Speed Situation*

Figure 8 shows the voltage and the current of the secondary side of the transformer. The current is in phase with the voltage and it was controlled to have an amplitude of 260A. The error between the real current and the reference current is shown in Figure 9.

The modulation voltage to activate the semiconductors on the single-phase side of the MMC is shown is Figure 10.

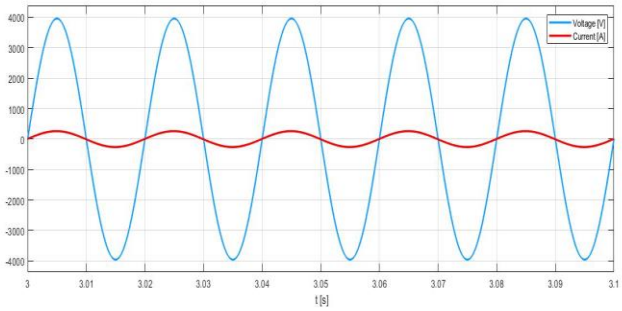

Figure 8 – Voltage and Current Fed into the MMC.

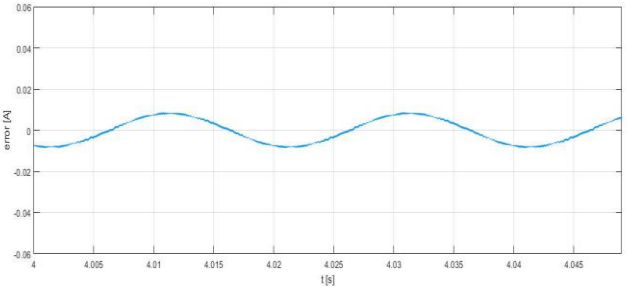

Figure 9 – Current Error.

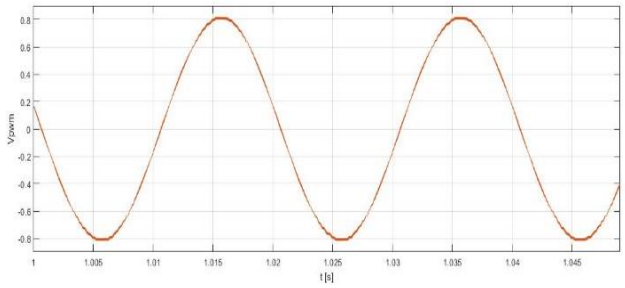

Figure 10 – PWM Signal.

Therefore, it is possible to represent the voltage in the positive (Figure 11) and negative (Figure 12) arms of the 1-φ branch of the MMC.

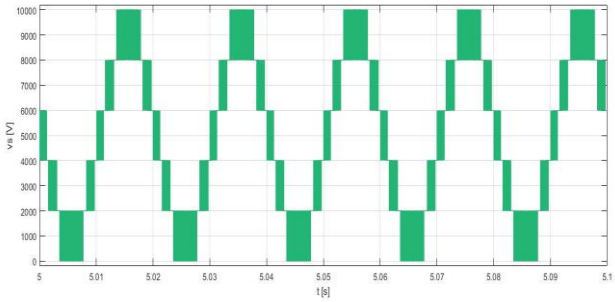

Figure 11 – Voltage of Upper Arm of MMC.

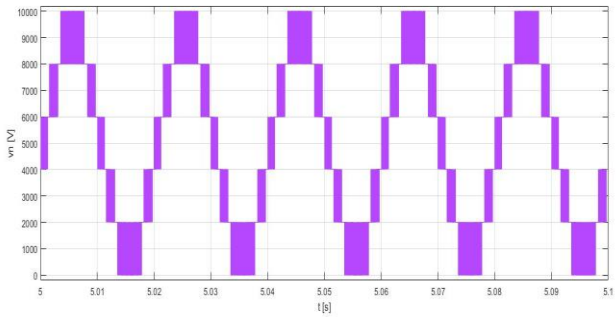

Figure 12 – Voltage of Lower Arm of MMC.

The 6 voltage levels in each arm can be noticed since they are composed by 5 submodules. Each level has 2kV of amplitude, represented by the constant voltage sources in each SM.

As previously mentioned, the SMs are using a half-bridge topology, therefore their IGBTs are complementarily driven. Figures 13 and 14 are showing the voltage and current of both devices during a very small period.

As the output of the MMC is connected to a three-phase induction motor, the semiconductors are activated to provide it a soft-start with a constant V/f relation. Figure 15 shows the 3 modulators with the same growth rate for voltage and frequency until their nominal values.

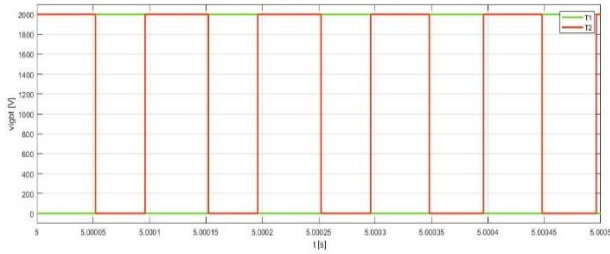

Figure 13 – IGBT Voltages from a Submodule.

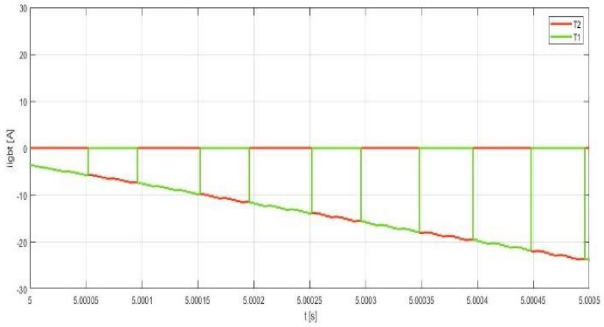

Figure 14 – IGBT Currents from a Submodule.

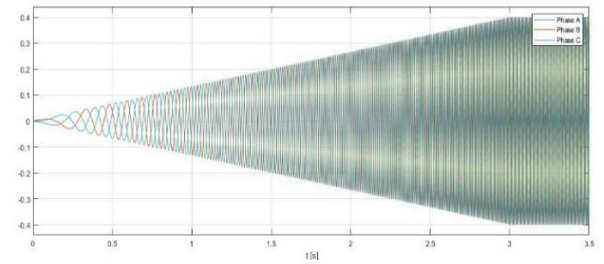

Figure 15 – Three-Phase Modulators of MMC.

The wave of the output voltage in one phase of the MMC is presented in Figure 16. There are less than 6 voltage levels since the modulators' amplitude was decreased to keep the motor fed by its nominal voltage.

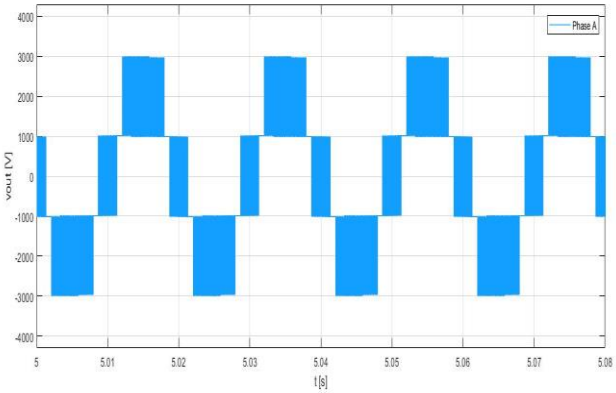

Figure 16 – Intermediate Voltage of a MMC Phase.

Figure 17 shows the $400V_{RMS}$ voltage applied to the motor. The currents are shown in Figure 18.

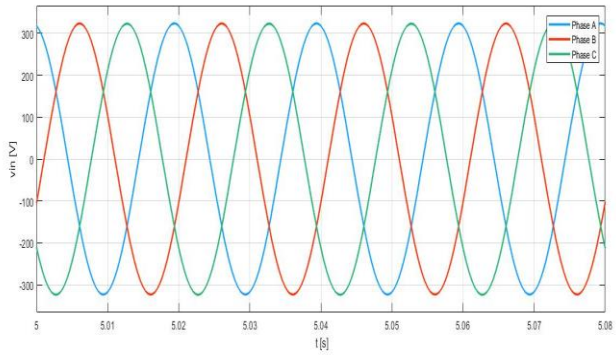

Figure 17 – Applied Voltage to the Motor.

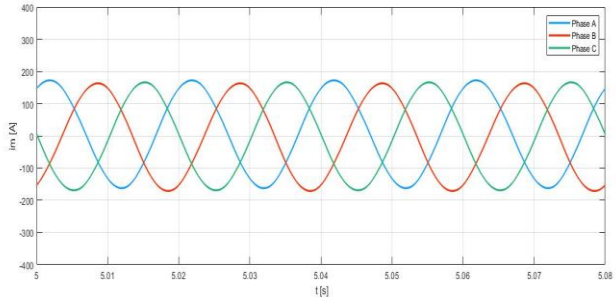

Figure 18 – Injected Current into the Motor.

The frequency reaches its nominal value within 3s. At this instant, a torque is applied to the motor. It linearly increases during 0.5s until reaches 176 Nm. This signal representation as well as the electromagnetic torque of the motor are shown in Figure 19.

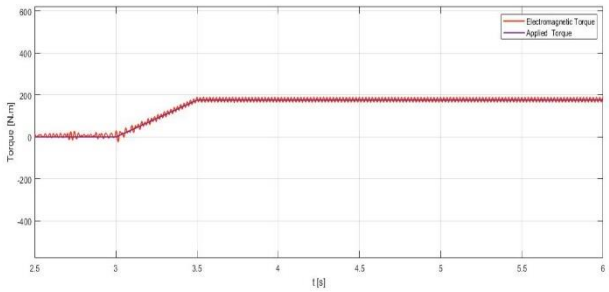

Figure 19 – Applied Torque and Electromagnetic Torque.

Figure 20 presents the motor speed in rpm. Its velocity increases for 3 seconds until it reaches its nominal value.

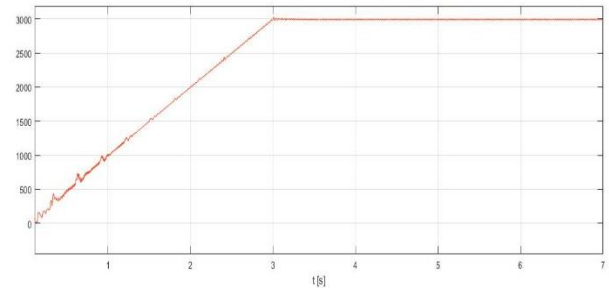

Figure 20 – Evolution of Motor Speed.

The currents in the stator can be seen in Figure 21. Their representation in steady state is shown in Figure 22.

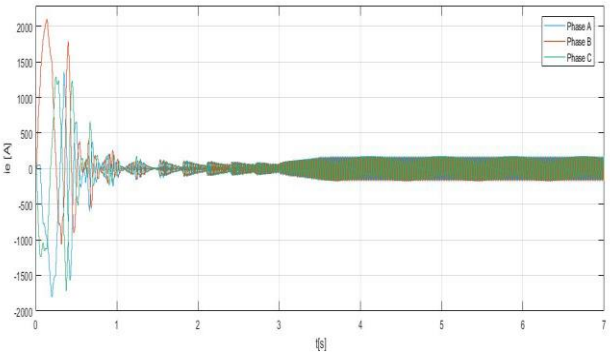

Figure 21 – Stator Current of the Motor.

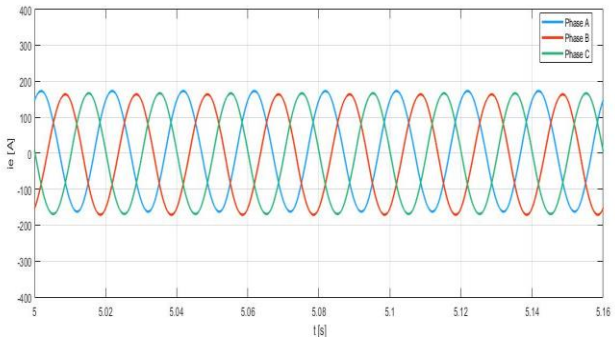

Figure 22 – Steady State Stator Current.

B. *Braking Situation*

This section presents the results of the braking simulation. To achieve this situation, some changes were done in the previous settings. Similarly to Figure 15, Figure 23 is showing the modulators of the three arms. After t=4s, the value of frequency and voltage are decreasing.

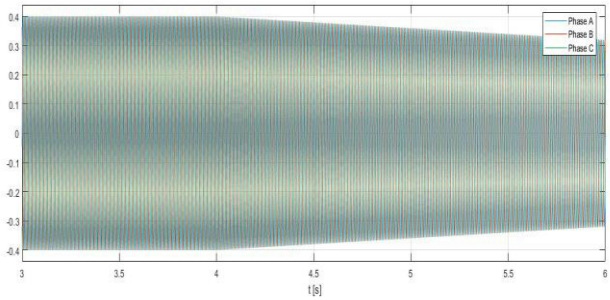

Figure 23 – New Modulators for Braking Application.

The applied torque is starting to decrease at t=4s and after 4.5 seconds it becomes negative until it stabilizes in -176Nm. The electromagnetic torque of the motor is represented in Figure 24 as well as the applied signal.

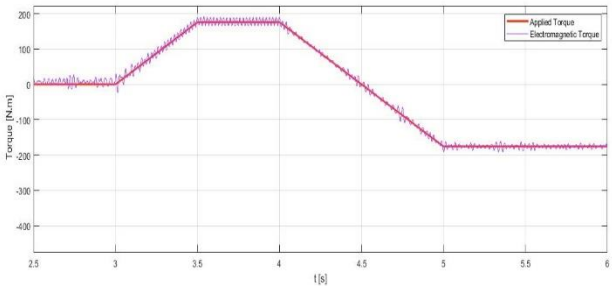

Figure 24 – New Applied Torque and Electromagnetic Torque.

Figure 25 shows the speed of the motor. Its value is reduced after t=4s, which confirms the braking of the train.

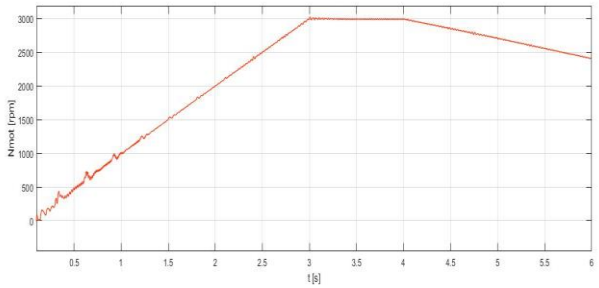

Figure 25 – Speed of the Motor with Braking.

Once the train is braking, the presence of recovered energy can be testified if the current is being delivered to the grid. Figure 26 shows the waveforms of the voltage and the current in the secondary side of the transformer.

Compared to Figure 8, the current is now shifted to the voltage by half-period. The fact that the current is being delivered to the grid proves that the motor is acting as a generator whilst the train is braking.

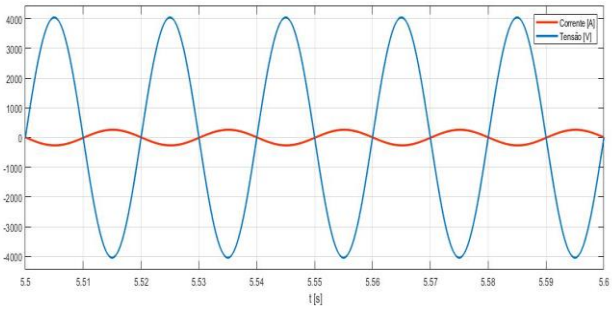

Figure 26 – New Current and Voltage from the Grid.

An advantage of the achieved regenerative braking is the operation of the motor below synchronous speed as it does not have constant frequency. The bidirectional feature of the MMC is also responsible to guarantee the changing of the current flow.

IV. CONCLUSIONS

The proposed on-board system was simulated and the graphical results were obtained to validate its operation. Firstly, a simulation was done considering positive acceleration of a train. The second simulation was performed with negative acceleration, which represents a braking scenario of the train.

The linear control of the grid current is implemented by a PI controller and the chosen modulation technique is the Phase-Shifted Carrier Pulse Width Modulation (PSC-PWM). It was possible to validate the controller feasibility by the small error between the real current and its reference.

For the designed MMC, its operation was validated by the number of voltage levels as well as the waveforms of current and voltage throughout its submodules. The three-phase arms of the MMC contributed to soft-start the motor with constant V/f relation preventing high starting currents through it.

Even though only 6 voltage levels were achieved, the peak voltage of the semiconductors was only 2kV. As the most advanced IGBTs are up to 6.5kV, the use of these new devices for the same number of voltage levels would work with a smaller traction transformer, that would need a lighter turn ratio. For more power in the converter, more levels could be implemented whereas the harmonic effect would be minimized.

Through the presented system it was possible to validate the regenerative braking, where the motor acts as a generator and the system delivers power back to the grid. The regenerative braking can occur below synchronous speed due to the frequency variation.

Therefore, the use of modular multilevel converters is essential for traction system applications especially due to their modularity and bidirectional features.

REFERENCES

[1] M. Plakhova, B. Mohamed, and P. Arboleya, "Static model of a 2×25kV AC traction system," in *2015 6th International Conference on Power Electronics Systems and Applications (PESA)*, Dec. 2015, pp. 1–5, doi: 10.1109/PESA.2015.7398916.

[2] I. Krastev, P. Tricoli, S. Hillmansen, and M. Chen, "Future of Electric Railways: Advanced Electrification Systems with Static Converters for ac Railways," *IEEE Electrif. Mag.*, vol. 4, no. 3, pp. 6–14, Sep. 2016, doi: 10.1109/MELE.2016.2584998.

[3] D. Ronanki and S. S. Williamson, "Modular Multilevel Converters for Transportation Electrification: Challenges and Opportunities," *IEEE Trans. Transp. Electrif.*, vol. 4, no. 2, pp. 399–407, Jun. 2018, doi: 10.1109/TTE.2018.2792330.

[4] D. Ramirez, F. Martinez-Rodrigo, S. de Pablo, and L. Carlos Herrero-de Lucas, "Assessment of a non linear current control technique applied to MMC-HVDC during grid disturbances," *Renew. Energy*, vol. 101, pp. 945–963, 2017, doi: 10.1016/j.renene.2016.09.050.

[5] F. Silva, S. Pinto, and J. Santana, *Conversores Comutados para Energias Renováveis*. 2016.

[6] S. Thamizharasan, J. Baskaran, S. Ramkumar, and S. Mubarak Ali, "Modified carrier PWM strategies for multilevel inverters," *Proc. Int. Conf. Comput. Power, Energy, Inf. Commun. ICCPEIC 2013*, vol. 49, no. 4, pp. 51–54, 2013, doi: 10.1109/ICCPEIC.2013.6778497.

[7] C. D. Townsend, T. J. Summers, and R. E. Betz, "Phase-Shifted Carrier Modulation Techniques for Cascaded H-Bridge Multilevel Converters," *IEEE Trans. Ind. Electron.*, vol. 62, no. 11, pp. 6684–6696, 2015, doi: 10.1109/TIE.2015.2442516.

[8] R. Darus, J. Pou, G. Konstantinou, S. Ceballos, and V. G. Agelidis, "A modified voltage balancing sorting algorithm for the modular multilevel converter: Evaluation for staircase and phase-disposition PWM," *Conf. Proc. - IEEE Appl. Power Electron. Conf. Expo. - APEC*, pp. 255–260, 2014, doi: 10.1109/APEC.2014.6803318.